2008

Application of the DSMC Method for Design of a Coaxial Microthruster Nozzle

William B. Stein
Purdue University

Alina A. Alexeenko
Purdue University - Main Campus, alexeenk@purdue.edu

44th AIAA/ASME/SAE/ASEE Joint Propulsion Conference & Exhibit
21 - 23 July 2008, Hartford, CT

AIAA 2008-4530

2008-4530

Joint Propulsion Conference, 21-23 July 2008, Hartford, CT

Application of the DSMC Method for Design of a Coaxial Microthruster Nozzle

William B. Stein*, and Alina A. Alexeenko†,
Purdue University, West Lafayette, IN 49707, U.S.A.

The Direct Simulation Monte Carlo (DSMC) method is used to numerically simulate and design a micronozzle with improved performance. Thrust calculations using the DSMC method demonstrate that the coaxial micronozzles can achieve milli-Newton thrust levels with specific impulses on the order of 45 s using argon in a cold gas expansion. Improved micronozzle designs of coaxial microthrusters are also proposed. Coaxial micronozzles utilizing center-body geometries to exploit pressure thrust show about 140% increase in specific impulse at low Reynolds numbers compared to a traditional converging nozzle.

Nomenclature

ν_m	Neutral Gas Collision Frequency	s^{-1}
τ_{coll}	Period Between Collisions	s
T_0	Stagnation Temperature	K
$\vec{F}$	External Force	N
α	Accommodation Coefficient	[ ]
$\bar{u}$,$\vec{v}$	Fluid Velocity	ms^{-1}
Δt	Time-step	s
Δx	Length-step	m
$\dot{m}$	Mass Flow Rate	kgs^{-1}
γ	Ratio of Specific Heats	[ ]
λ	Mean Free Path	m
μ_{ref}	Reference Viscosity	$Nm^{-2}s$
ρ	Mass Density	kgm^{-3}
τ_{res}	Particle Residence Time within a Cell	s
$\vec{x}$	Position Vector	m
A^*	Throat Area	m^2
C_D	Mass Discharge Coefficient	[ ]
D_{th}	Throat Diameter	m^2
F	Thrust	N
F_c	Cold Gas Thrust	N
F_{cb}	Pressure Thrust, Center-Body	N
F_{jet}	Jet Thrust	N
F_{jp}	Pressure Thrust, Jet	N
F_{np}	Pressure Thrust, Nozzle Back Face	N
g	Acceleration of gravity	ms^{-2}
I_{sp}	Specific Impulse	s

*Ph.D. Candidate, School of Aeronautics and Astronautics, E-mail: steinw@purdue.edu, AIAA Student Member.
†Assistant Professor, School of Aeronautics and Astronautics, E-mail: alexeenk@purdue.edu, AIAA Member

m	Molecular Mass	kg
N_c	Number of Particles per Computational Cell	[ ]
n_g	Number Density	m^{-3}
P	Pressure	$Torr$
P_c	Chamber Pressure	$Torr$
P_0	Stagnation Pressure	$Torr$
$PFnum$	Number of Molecules Represented by a Computational Particle	[ ]
Q	Volumetric Flow Rate	$sccm$
R	Gas Constant	$Jkg^{-1}K^{-1}$
T	Temperature	K
T_x	Component of Translational Temperature in x-direction	K
v	Velocity	ms^{-1}
v_r	Relative Velocity	ms^{-1}

I. Introduction

Microthrusters are becoming increasingly important onboard modern microspacecraft. While many spacecraft systems can be miniaturized with the application of new technology, hardware limitations and power requirements still constrain traditional propulsion system size. Thus, many of today's micro- and nanosatellites have no onboard propulsion capabilities, even though these smaller spacecraft have similar mission requirements of traditional satellites. The number of nanosatellite ($<$ 20 kg) launches per year has accelerated over the past decade.[1] Some of these satellites (SNAP-1)[2] utilize cold gas thrusters for orbital insertion only, with no provisions for attitude control or station keeping. The upcoming LISA mission will utilize higher precision cold gas thrusters for formation flying missions,[3] and while thruster candidates are available, no cold gas thruster has demonstrated the performance or lifetime requirements.

Chemical propulsion systems commonly use converging-diverging *de Laval* nozzles in high Reynolds number flows to efficiently convert a higher pressure into kinetic energy and provide thrust. Traditional space propulsion systems typically operate with high exhaust velocities and moderate to large length scales, resulting in very high Reynolds numbers. Thus, viscous effects are small and the flow can be approximated as largely inviscid. For low Reynolds number flows, a simple orifice has comparable performance to a converging-diverging nozzle.[4,5]

Developing supersonic micronozzles present difficult design challenges when compared to larger nozzles.[6,7] Micronozzles have much smaller length scales ($mm - \mu m$) and thus the corresponding Reynolds numbers are low ($Re < 500$), reducing nozzle performance.[5] In micronozzles, it is not uncommon for the viscous boundary layer to occupy a sizeable portion of the flow cross-section within the nozzle. Heat transfer within the micronozzles becomes problematic as the thermal mass of the flow is reduced and the surface-to-volume ratio increases. Also, rarefied effects become a concern as the mean free path of the fluid approaches that of the characteristic length scales of the micronozzle. To reduce viscous effects within the micronozzle, an alternative concept is investigated.

Aerospike and plug nozzles have been historically used with higher Reynolds number systems in the past.[8,9] The main advantage of this type of nozzle resides in its pressure compensating ability. The lack of an enclosed divergent section allows the flow to conform more freely to the ambient pressure, thus improving performance over a range of pressure conditions. While this is advantageous for larger nozzles, pressure compensation is not a major concern of micronozzle design, since most micronozzles operate specifically in a vacuum. However, utilizing a center-body for expansion provides the ability to reduce the surface area of the nozzle and thus reducing viscous losses.[10]

Another possible means of increasing the nozzle performance is to utilize pressure thrust more effectively. Due to the operating environment of microthrusters and their thrust levels, the pressure thrust component can be a significant portion of the overall thrust. While it is understood that viscous losses dominate low Reynolds number flow, little information is present on designing a microthruster nozzle which better utilizes

pressure thrust itself to improve performance. Thus, a more efficient micronozzle is sought using DSMC simulations. The baseline nozzle geometry studied here correspond to the RF plasma thruster studied experimentally.[11,12] The main goal of this investigation is to develop a more efficient micronozzle using DSMC simulations.

II. Direct Simulation Monte Carlo Model

The Direct Simulation Monte Carlo (DSMC) method[13] is applied to model the neutral gas expansion in the microthruster nozzle. This type of approach is required due to significant rarefaction of the flow within the operating pressure range (mTorr -Torr) of the nozzle. The value of the Knudsen number based on an orifice diameter of 2 mm is about 0.04 at $P = 1$ Torr and $T = 300$ K, and increases for higher temperatures and lower pressures.

The 2-D, axisymmetric DSMC code SMILE[14] was used to simulate neutral, unreacting flow through the micronozzle and into vacuum. An ensemble of computational particles is created by dividing the total number of physical particles by $PFnum$. This method also discretizes the spatial coordinates of the nozzle into cells and utilizes discrete time-steps. The cells are used to sample flow properties and the gas state by averaging the molecular properties within each cell as well as for the implementation of the collisional relaxation process.

During each full time-step, two processes occur: molecular free flight and binary collisions. The molecular free flight step updates the positions of every particle by computing their new positions via their velocity and the time-step used

$$\vec{x}_i(t + \Delta t) = \vec{x}_i(t) + \vec{v}_i \cdot \Delta t \tag{1}$$

where $\vec{x}_i$ and $\vec{v}_i$ are position and velocity of the i^{th} particle. Model particles are also accelerated by any external forces present, $\vec{F}$.

$$\vec{v}_i(t + \Delta t) = \vec{v}_i(t) + \frac{\vec{F}}{m} \cdot \Delta t \tag{2}$$

Once the new positions of the particles are known, the number of binary collisions is calculated. Binary collisions are modeled using a two step process. First, an appropriate number of collisions are sampled within the cell. Then the post-collisional velocities of each collisional pair is sampled. The time between consecutive collisions is determined and the time between collisions is sampled using the acceptance-rejection method using a maximum collision frequency

$$\nu_m = \frac{N_c(N_c - 1)}{2} \frac{PFnum}{V_c} [\sigma(v_r)v_r)]_{max} \tag{3}$$

$$v_r = |\vec{v}_i - \vec{v}_j| \tag{4}$$

where N_c is the number of model particles in a cell with a volume V_c, v_r is the magnitude of the relative velocity between particles i and j, and $\sigma(v_r)$ is the collision cross-section which depends on a specified binary interaction potential.

After each time-step, particles are injected through designated boundaries and collisions/interactions with solid surfaces occur. This model utilizes the specular/diffuse Maxwell gas-surface interaction model. This interaction model assumes that only a fraction $(1 - \alpha)$ of particles colliding with a surface reflect specularly while the remaining particles reflect diffusely. Particles which diffusely reflect acquire velocities which are distributed using a Maxwellian distribution corresponding to the wall temperature. α is also referred to as the tangential momentum accommodation coefficient. A similar procedure can be performed using an energy accommodation coefficient to determine how a collision with a surface affects the energy of a particle as well. Simulations in this investigation also utilize a variable hard sphere model, a molecular diameter of 4.17×10^{-10} m and a viscosity-temperature exponent $\alpha_v = 0.31$ for argon. The computational parameters of the DSMC model were chosen to meet the following criteria for numerical accuracy:

- Time-step: $\Delta t \leq min\{\tau_{coll}, \tau_{res}\}$

- Cell Size: Cell size should be smaller than the local mean free path, λ
- Ratio of Computational to Physical Particles: Determined such that $PFnum$ results in $\gtrapprox 5$ computational particles per cell on average, and $\gtrapprox$ least 1 computational particle per cubic mean free path

$$\tau_{coll} = \frac{\lambda}{v} \tag{5}$$

$$\tau_{res} = \frac{\Delta x}{v} \tag{6}$$

Subsonic boundary conditions are imposed implicitly via a local average of flow properties[15–18] at a control surface. Specifically, the inlet velocity is set to an average of the flow velocity in the adjacent cells. A control surface is placed immediately downstream of the inflow boundary. The inflow boundary conditions are updated every 100 timesteps. The nozzle flow is simulated until the steady state is reached and the macroscopic flow parameters are then calculated.

The micronozzle performance parameters such as thrust, mass flow rate and specific impulse are calculated based on the DSMC solution. This is compared with the performance of a cold gas expansion for the same geometry and similar operating conditions. For non-equilibrium flow, the jet thrust can be found as the momentum flux at the nozzle exit as[19]

$$F_{jet} = \int_A \rho \left\{ \int_a^b \int_{-\infty}^{\infty} \int_0^{\infty} u^2 f du dv dw \right\} dA = \int_A \left(\rho \bar{u}^2 + P \frac{T_x}{T} \right) dA \tag{7}$$

where u, v, w are molecular velocity components, $f = f(\vec{x}, \vec{v})$ is the velocity distribution function and T_x is the axial temperature component which differs from the overall translational temperature in nonequillibrium flows. The total thrust can then be calculated as

$$F = F_{jet} + R_x \tag{8}$$

The second terms in the above equation is the resultant force in the x-direction due to pressure and shear stress on any external surface of the nozzle.

Theoretical microthruster performance for the converging nozzle can be estimated assuming isentropic expansion into vacuum as

Continuum Flow through a Smooth Sonic Nozzle:

$$\dot{m} = \left(\frac{2}{\gamma + 1} \right)^{\frac{\gamma+1}{2(\gamma-1)}} \sqrt{\frac{\gamma}{RT_0}} P_0 A^* \tag{9}$$

$$gIsp = \sqrt{\frac{2RT_0(\gamma + 1)}{\gamma}} \tag{10}$$

Free Molecular Orifice Flow:

$$\dot{m} = \left(\frac{1}{\sqrt{2\pi RT_0}} \right) (P_0 - P_a) A^* \tag{11}$$

$$gI_{sp} = \frac{1}{2} \sqrt{2\pi RT_0} \tag{12}$$

III. Micronozzle Design

Four general categories of micronozzle designs were considered in this study. Each of these categories deviate from the baseline design in a related fashion. The baseline nozzle design was based on an actual experimental nozzle used with the RF plasma thruster at Purdue[11,12] and consists of a converging conical nozzle with a sharp orifice. A schematic of the baseline nozzle and flowfields for the are shown in Figure 1. Convergence in terms of DSMC parameters was analyzed by increasing the number of computational particles and decreasing the timestep. Both these cases varied from the original baseline simulation by only a few percent. Simulation results are then compared with a baseline converging nozzle and are presented in Table 1.

Table 1. DSMC Convergence Study for a Baseline Micronozzle, (5.2 Torr Chamber Pressure, 3.175 mm Inner Radius)

Case	$\dot{m}$ [mg/s]	F [mN]	F_{jet} [%]	F_{jp} [%]	F_{np} [%]	I_{sp} [s]	Improvement over Baseline [%]
Baseline	0.959	0.435	53.8	45.1	0.95	46.2	-
Particles Doubled	0.950	0.421	54.3	44.9	0.76	45.2	-2.17
Half Timestep	0.924	0.420	54.5	44.8	0.80	46.4	0.42
Computational Parameters							
	Particles $\times 10^6$		Collision Cells $\times 10^6$		Molecules per λ^3		# Collisions per Timestep per Molecule
Baseline	4.2		1.4		1.66		0.51
Particles Doubled	8.1		2.2		3.31		0.73
Half Timestep	4.0		1.3		1.66		0.35

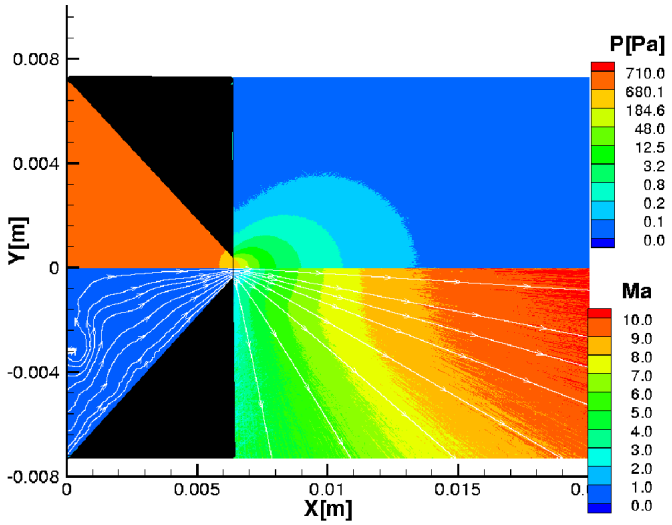

Figure 1. Baseline Micronozzle Performance: DSMC Calculated Pressure Contours (top, [Pa]), Mach Number Contours, and Streamlines (Bottom) for Baseline Nozzle Geometry.

The baseline nozzle flow can be divided into three major regions: the convergent section, the throat, and the divergent section. Categories of nozzle designs were created with the intention of investigating geometry effects of each of these sections on micronozzle performance. This is done by comparing each micronozzle specific impulse to the baseline design, with an aim of achieving a relative performance increase. The specific impulse of each nozzle is calculated as the ratio of the total generated thrust to the massflow. It should

be noted that the total generated thrust for a micronozzle operating at these conditions is comprised of three terms. The first two terms are the traditional jet and pressure thrust terms derived from momentum conservation of the fluid as it leaves the nozzle. An additional term is required which determines the resultant pressure thrust integrated over the entire external surface of the nozzle (See Equation 8). Since this micronozzle operates in vacuum and at such low thrust levels, any pressure present on the back face of the nozzle, F_{np}, can produce a non-trivial amount of thrust. Typical values of F_{np} range on the order of a few percent of the total thrust for nozzle designs without divergent section, but can become much larger using other geometries, for example, with a center-body.

The first category of micronozzles considered are obtained by the addition of a divergent section of the nozzle or by using a simple orifice to choke the flow. Table 2 shows calculated performance for this category of nozzles. It can be seen that a symmetric converging-diverging nozzle provides about a 3% increase in nozzle performance, while an orifice can provide about a 2% increase. The converging-diverging nozzle shown in Figure 2(a) shows a uniform expansion through the diverging section of the nozzle with a sonic line slightly downstream of the throat. Figure 2(b) illustrates the orifice flowfield and has a sonic line within the orifice. The converging-diverging nozzle acheives higher Mach numbers and has higher pressures acting along the wall of the diverging section of the nozzle when compared to the orifice.

Table 2. Micronozzle Performance for Traditional Nozzle Variations, (5.2 Torr Chamber Pressure, 3.175 mm Inner Radius)

Case	Re	$\dot{m}$ [mg/s]	F [mN]	F_{jet} [%]	F_{jp} [%]	F_{np} [%]	I_{sp} [s]	Improvement over Baseline [%]
Baseline	72.1	0.959	0.435	53.8	45.1	0.95	46.2	-
Orifice	50.8	0.597	0.276	68.8	29.6	1.53	47.2	2.16
Con.-Div.	70.9	1.098	0.513	91.7	8.34	1.00	47.2	3.27

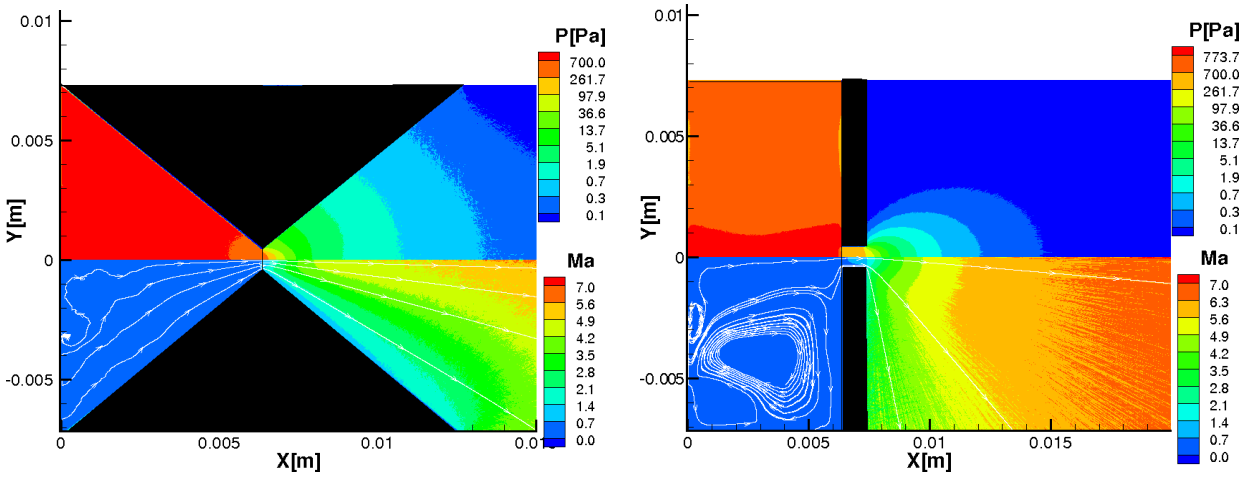

(a) Converging-Diverging Nozzle Flow Field (b) Orifice Flow Field

Figure 2. DSMC Calculated Pressure Contours (Top, [Pa]), Mach Number Contours and Streamlines (Bottom) for Traditional Nozzles

The second category of nozzle designs consists of changes in the throat diameter of the micronozzle. The original experimental nozzle used no means to size the throat and was set sufficiently small to ensure choking. Thus, this category of micronozzle designs attempts to investigate how changing the throat diameter may improve micronozzle performance. This was achieved by increasing and decreasing the throat diameter for a similar converging geometry and observing the effect on performance. Figures 3(a) and 3(b) illustrate that the current nozzle diameter can be increased to further improve performance, with Figure 3(b) showing more uniform flow through the nozzle. Increasing the throat diameter reduces boundary layer effects and

increases the throat Reynolds number. Micronozzle performance also decreases if the diameter becomes too large, thus illustrating there is an optimum nozzle diameter between about 3.33 mm and 6.60 mm. While this may be said, optimizing the throat diameter provides little benefit in terms of performance for this type of nozzle, generally resulting in a change of $\approx \pm 1\%$ which is on the order of statistical noise.

Table 3. Micronozzle Performance for Different Throat Diameters, (5.2 Torr Chamber Pressure, 3.175 mm Inner Radius)

Case	Re	$\dot{m}$ [mg/s]	F [mN]	F_{jet} [%]	F_{jp} [%]	F_{np} [%]	I_{sp} [s]	Improvement over Baseline [%]
Baseline	72.1	0.959	0.435	53.8	45.1	0.95	46.2	-
Half Throat	35.0	0.229	0.106	51.3	42.4	6.26	47.2	2.32
2x Throat	144	3.89	1.72	54.1	45.5	0.43	45.2	-2.19
4x Throat	272	14.8	6.67	53.8	46.0	0.266	45.9	-0.64
8x Throat	456	50.5	22.1	54.9	45.0	0.109	44.6	-3.50

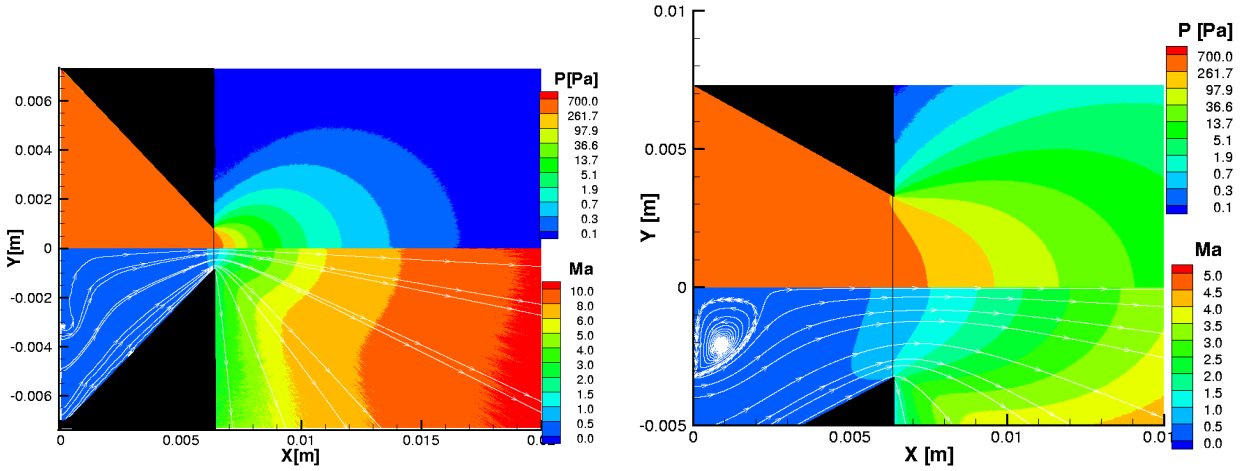

(a) 2x Throat Diameter Flow Field

(b) 8x Throat Diameter Flow Field

Figure 3. DSMC Calculated Pressure Contours (Top, [Pa]), Mach Number Contours and Streamlines (Bottom) for Various Throat Diameters

The third category investigates flow characteristics within the convergent section of the micronozzle. This category explored the possibility of reducing the impact of the recirculation region due to flow separation off the inner electrode as it leaves the discharge chamber (shown in Figure 1). Three geometries were investigated: one with a small decrease in turning angle, with the inner electode and nozzle walls parallel, and with the inner electrode extending into the throat itself. Schematics of these designs are given in Figure 4. None of these designs produced the desired effect and, in fact, tended to reduce performance. This can be attributed to the relatively low velocities with respect to the throat velocity and increases in boundary layer thickness within the nozzle throat, thus reducing performance.

The last category considers nozzles with a center-body added externally to a converging nozzle. Flow field results are shown in Figures 5 and 6 which show remarkably improved performance ($> 110\%$) over the baseline design. It should be noted that the distance between the inner plug and the convergent section of the nozzle was sized such that it is the same as the radius of the baseline case. Thus, these nozzles should be more appropriately compared with the *half-throat* micronozzle which has a similar Reynolds number, but wasn't deemed a concern due to the small performance difference between the *half-throat* and *baseline* cases. These nozzles have an "annular" design which better utilizes the flow geometry present in a coaxial electrode arrangement. The nozzle provides a smooth transition between the discharge chamber and the nozzle throat,

Table 4. Micronozzle Performance for Convergent Section Variations, (5.2 Torr Chamber Pressure, 3.175 mm Inner Radius)

Case	Re	$\dot{m}$ [mg/s]	F [mN]	F_{jet} [%]	F_{jp} [%]	F_{np} [%]	I_{sp} [s]	Improvement over Baseline [%]
Baseline	72.1	0.959	0.435	53.8	45.1	0.95	46.2	-
Conv. Nozzle 1	70.0	0.931	0.424	53.0	45.0	2.02	46.4	0.54
Conv. Nozzle 2	70.7	0.941	0.428	53.5	44.5	2.01	46.4	0.47
Conv. Nozzle 3	59.5	0.868	0.390	52.6	45.3	1.92	45.7	-0.93

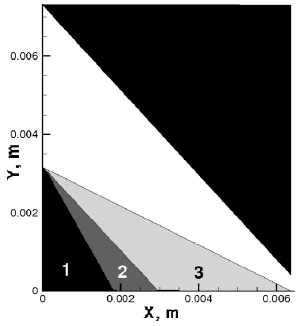

Figure 4. Nozzle Schematics for Converging Nozzle Cases

Table 5. Micronozzle Performance for Center-body Geometries, (5.2 Torr Chamber Pressure, 3.175 mm Inner Radius)

Case	Re	$\dot{m}$ [mg/s]	F [mN]	F_{jet} [%]	F_{jp} [%]	F_{np} [%]	F_{cb} [%]	I_{sp} [s]	Improv. over Baseline [%]
Baseline	72.1	0.959	0.435	53.8	45.1	0.95	-	46.2	-
Annular Nozzle	29.2	0.825	0.874	25.9	15.2	3.09	56.2	108	134
Conical 30 °	28.5	0.813	0.652	33.8	20.9	4.93	40.4	81.8	77.1
Conical 60 °	28.9	0.813	0.882	25.4	14.9	3.26	56.6	111	140
Biconical 60 ° − 30 °	28.8	0.814	0.886	25.3	14.9	3.10	56.7	111	140

without any flow separation. Due to the annular configuration, as the flow leaves the nozzle throat, it creates a recirculation region outside the nozzle itself. While this would be detrimental and most likely reduce nozzle performance under other circumstances (higher thrust levels or expanding into atmospheric conditions for example) this stagnation region produces an additional pressure thrust in the case of expansion into vacuum at low Reynolds numbers.

As the flow exits the annular nozzle, it expands into itself along the centerline of the nozzle causing a "high pressure" region on the order of 0.25 Torr along the center-body compared to 0.02 Torr on the upper face of the nozzle. This creates about 0.5 mN of additional pressure thrust in vacuum. While the magnitude of the center-body thrust is small, it is large relative to the total thrust provided by the micronozzle itself ($\approx 50\%$), and thus would not improve the performance of larger thrust nozzles.

The four nozzle designs in this category explore different half-angles of the center-body in order to better exploit this additional pressure thrust. Figures 5 and 6 illustrate that nozzles with a higher half-angle, and thus more blunt, exploit the additional pressure thrust better than longer center-bodies with a smaller half-angle. Also, an annular nozzle with a flat center-body has reduced performance with respect to that of a large half-angle center-body. Further design may be implemented to better optimize micronozzles of this type to increase micronozzle performance.

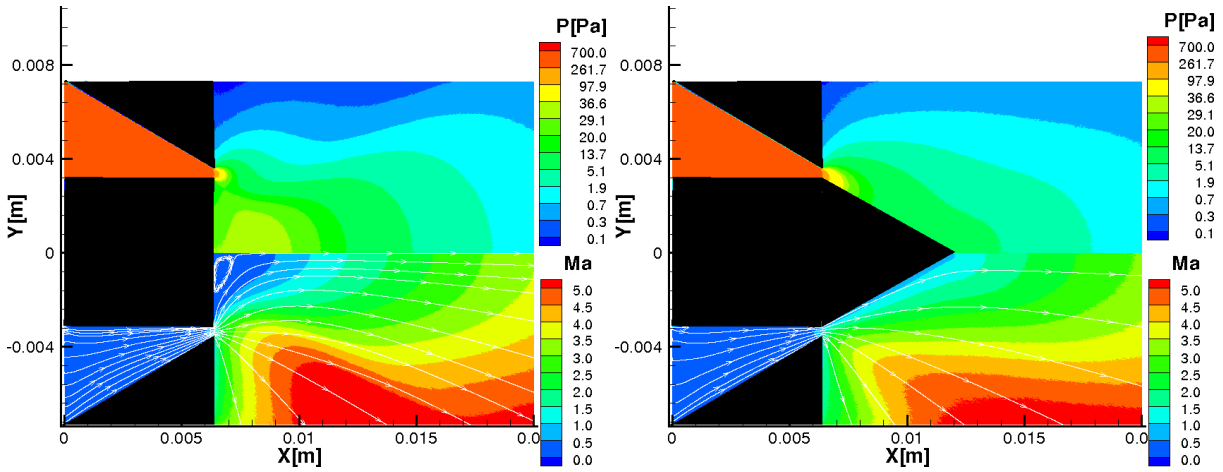

(a) Annular Nozzle Field

(b) 30^0 Conical Center-Body

Figure 5. Center-Body Micronozzles: DSMC Calculated Streamlines and Pressure (top) and Mach Number (bottom) Contours

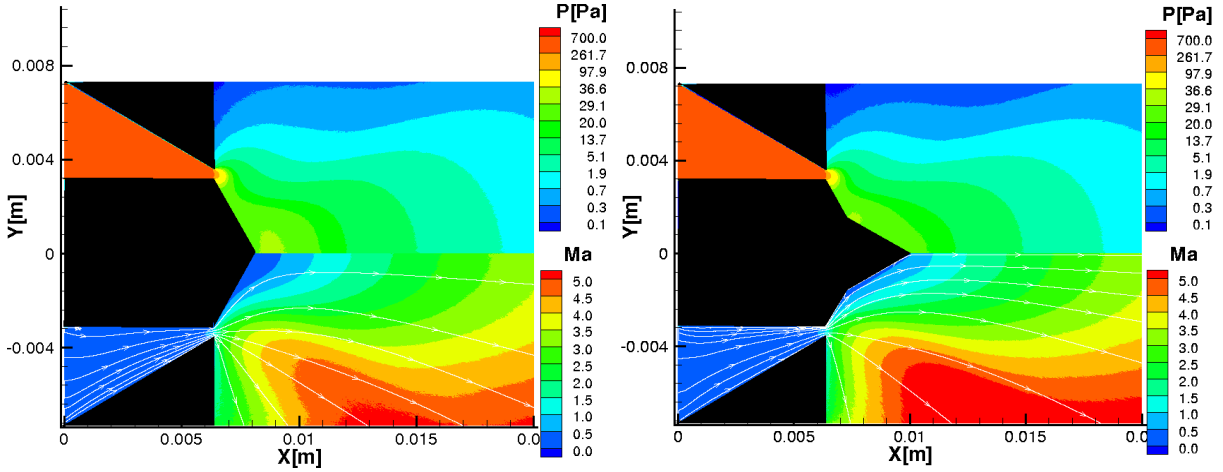

(a) 60^0 Conical Center-Body

(b) $60^0 - 30^0$ Biconical Center-Body

Figure 6. Center-Body Micronozzles: DSMC Calculated Streamlines and Pressure (top) and Mach Number (bottom) Contours

IV. Conclusions

This investigation shows that coaxial micronozzle concepts using center-body geometries can potentially provide thrust in the milli-Newton range while achieving significant improvements in specific impulse compared to typical converging nozzle cold gas thrusters. Changes in throat diameter, the geometry of the converging section and the addition of a diverging section provide little improvement over a comparable converging nozzle at these operating conditions. The addition of blunt center-bodies increases the pressure thrust due to the creation of a recirculation/stagnation zone aft of the center-body. This increase in pressure thrust is of the same magnitude as the jet thrust, thus nearly doubling the thrust level for the same mass flow rate. Short center-bodies perform better than longer center-bodies due to a reduction in viscous losses and better capture of the flow expansion. This performance improvement is only applicable at low Reynolds numbers, low thrust, vacuum conditions and would not provide any additional benefit for nozzles operating

at larger thrust levels, within the atmosphere, or at high Reynolds numbers.

Acknowledgments

The computations reported in this paper were performed on 16 CPU Sunfire 4600 awarded through Sun Microsystems, Inc. Academic Excellence Grant award #EDUD-7824-070336-US.

References

[1]Caceres, M., "The emerging nanosatellite market," *Aerospace America*, February 2001, pp. 16–18.

[2]Baker, A. and Underwood, C., "Micropropulsion from Snap to PALMSAT: When Does MEMS Become the Way Forward?" *Proceedings of NanoTech 2002 - "At the Edge of Revolution", AIAA-2002-5759, Houston, TX*, Sept. 2002.

[3]Ziemer, J. and Merkowitz, S., "Microthrust Propulsion for the LISA Mission," *40th Joint Propulsion Conference*, 2004, AIAA Paper 2004-3439.

[4]Lily, T., Gimelshein, S., Ketsdever, A., and Markelov, G., "Measurements and Computations of Mass Flow and Momentum Flux through Short Tubes in Rarefied Gases," *Physics of Fluids*, Vol. 18, No. 093601, 2006, pp. 1–11.

[5]Jamison, A. and Ketsdever, A., "Performance Comparison of Underexpanded Orifices and DeLaval Nozzles at Low Reynolds Numbers," *38th Joint Propulsion Conference*, 2002, AIAA Paper 2002-3690.

[6]Louisos, W., Alexeenko, A., Hitt, D., and Zilic, A., "Design Considerations for Supersonic Micronozzles," *International Journal of Manufacturing Research*.

[7]Ketsdever, A. and Mueller, J., "Systems Considerations and Design Options for Microspacecraft Propulsion Systems," *35th AIAA Joint Propulsion Conference*, 1999, AIAA Paper 99-2723.

[8]Marcum, D. and Hoffman, J., "Calculation of Three-Dimensional Inviscid Flowfields in Propulsive Nozzles with Centerbodies," *24th AIAA Aerospace Sciences Meeting*, 1986, AIAA Paper 86-0449.

[9]Migdal, D., "Supersonic Annular Nozzles," *Journal of Spacecraft*, Vol. 9, No. 1, 1972.

[10]Zilic, A., Hitt, D., and Alexeenko, A., "Numerical Simulations of Supersonic Flow in a Linear Aerospike Micronozzle," *37th AIAA Fluid Dynamics Conference and Exhibit*, 2007, AIAA Paper 2007-3984.

[11]Hrbud, I., Kemp, G. E., Yan, A. H., and Gedrimas, J. G., "Review of RF Plasma Thruster Development," *IEPC Paper 2007-309*, 2007.

[12]Stein, W., *Performance Characterization of a Radio Frequency Capacitively Coupled Discharge Microthruster*, Ph.D. thesis, Purdue University, 2008.

[13]Bird, G., *Molecular Gas Dynamics and the Direct Simulation of Gas Flows*, Oxford University Press, 2004.

[14]Ivanov, M., Kashkovsky, A., Gimelshein, S., Markelov, G., Alexeenko, A., Bondar, Y., Zhukova, G., Nikiforov, S., and Vaschenkov, P., "SMILE System for 2D/3D DSMC Computations," *Proceedings of 25th International Symposium on Rarefied Gas Dynamics*, 2006.

[15]Alexeenko, A., Gimelshein, S., and Levin, D., "Reconsideration of Low Reynolds Number Flow-Through Constriction Microchannels Using the DSMC Method," *Journal of Microelectromechanical Systems*, Vol. 14, No. 4, 1996.

[16]Alexeenko, A., Levin, D., Gimelshein, S., Collins, R., and Markelov, G., "Numerical Simulation of High Temperature Gas Flows in a Millimeter-Scale Thruster," *Journal of Thermophysics and Heat Transfer*, Vol. 16, No. 1, 2002, pp. 10–19.

[17]Piekos, E. and Breuer, K., "Numerical Modelling of Micromechanical Devices Using the Direct Simulation Monte Carlo Method," *Journal of Fluids Engineering*, Vol. 118, 2005.

[18]Fang, Y. and Liou, W., "Computations of the Flow and Heat Transfer in Microdevices Using DSMC with Implicit Boundary Conditions," *Journal of Heat Transfer*, Vol. 124, 2002.

[19]Alexeenko, A., Gimelshein, S., Levin, D., Ketsdever, A. D., and Ivanov, M., "Measurements and Simulation of Orifice Flow for Micropropulsion Testing," *Journal of Propulsion and Power*, Vol. 19, No. 4, 2003, pp. 588–594.